Hindawi
Journal of Nanomaterials
Volume 2019, Article ID 2820962, 7 pages
https://doi.org/10.1155/2019/2820962

Research Article

Electrochemical Epitaxial Growth of TiO_2/CdS/PbS Nanocables

Peng Wang,[1,2] Zhongyang Zhang,[3] Hua Wang,[4] Tieqiang Zhang,[3] Haining Cui,[3] Yue Yang,[1] and William W. Yu[1,4]

[1]*State Key Laboratory on Integrated Optoelectronics, College of Electronic Science and Engineering, Jilin University, Changchun 130012, China*
[2]*College of Materials Science and Engineering, Beijing University of Technology, Beijing 100124, China*
[3]*State Key Laboratory of Superhard Materials, College of Physics, Jilin University, Changchun 130012, China*
[4]*Department of Chemistry and Physics, Louisiana State University, Shreveport, LA 71115, USA*

Correspondence should be addressed to Yue Yang; yangyue@jlu.edu.cn and William W. Yu; wyu6000@gmail.com

Received 7 February 2019; Accepted 3 April 2019; Published 30 April 2019

Guest Editor: Jamal Siddiqui

Electrochemical deposition as a liquid phase epitaxial growth method is widely used to fabricate different kinds of hierarchical structures. As a typical heterostructure, TiO_2/PbS is widely utilized in the areas of photovoltaics and photocatalysis. Oriented TiO_2 nanorod (NR) arrays can provide direct pathways for the electron transport of photoanode. However, the lattice mismatch between TiO_2 NR sides and PbS is very large; PbS nanoparticles (NPs) only formed on the top of TiO_2 NRs. To solve this problem, TiO_2/CdS core/shell nanocables were firstly prepared electrochemically because the lattice ratio between TiO_2 and CdS was 0.916; and then, PbS NPs were successfully deposited over CdS shells (the lattice ratio between CdS and PbS was 0.697) to form TiO_2/CdS/PbS hierarchical heterostructures. Experimental results demonstrated that the CdS interlayer could effectively promote the growth of PbS NPs on the surface and improve the fill factor and short current density of the photoanodes.

1. Introduction

Various heterostructures have been utilized in the areas of photovoltaics [1–5] and photocatalysis [6, 7], such as CdS [8, 9], CdSe [10, 11], CdTe [12], PbS [2, 13], PbSe [14–18], and AgSe [19] over the surface of TiO_2 [20–22] and ZnO [23–25], with different morphologies such as multilayered films, core/shell nanocables, and spherical dots. Several different chemical methods, including electrochemistry [12, 26, 27], chemical bath deposition (CBD) [28, 29], assembly of quantum dots (QDs) by immobilization via organic linkers [30], and successive ionic layer adsorption and reaction (SILAR) [31, 32], are commonly used to fabricate these heterostructures. Among them, electrochemistry as a liquid-phase epitaxial growth method is easy to fabricate large-area devices with facile and labor-saving superiorities, particularly on nanorod (NR) arrays.

As one of these typical heterostructures, the TiO_2/PbS heterostructure has already been widely studied. Chen and coworkers used bath deposition to fabricate a TiO_2/PbS counter electrode for QD-sensitized solar cells [33]. Mali et al. fabricated solar cells via SILAR [34]. Sargent's group utilized colloidal PbS QDs to form heterostructure solar cells [35, 36]. But the separation of the photocarriers in these structures often does not do well due to the low lattice ratio.

Here, we tried to electrically deposit PbS over TiO_2 NR arrays which could provide direct pathways for photoelectron transporting from the points of injection at the interfaces of the heterostructures between the two different materials to the transparent conducting oxide (TCO) electrodes. However, we found that PbS nanoparticles (NPs) were only grown on top of the TiO_2 NRs due to the low lattice ratio between the sides of TiO_2 NR and PbS (about 0.495), so fully covered TiO_2/PbS heterostructures were not realized. CdS/PbS heterostructures are also widely used in the area of photovoltaics [37, 38]. In this work, we coated a layer of CdS over TiO_2 NRs by electrochemistry because the lattice ratio between TiO_2 nanorod and CdS is only 0.916. Then, PbS QDs were deposited on the surfaces of core/shell TiO_2/CdS nanocables to form TiO_2/CdS/PbS

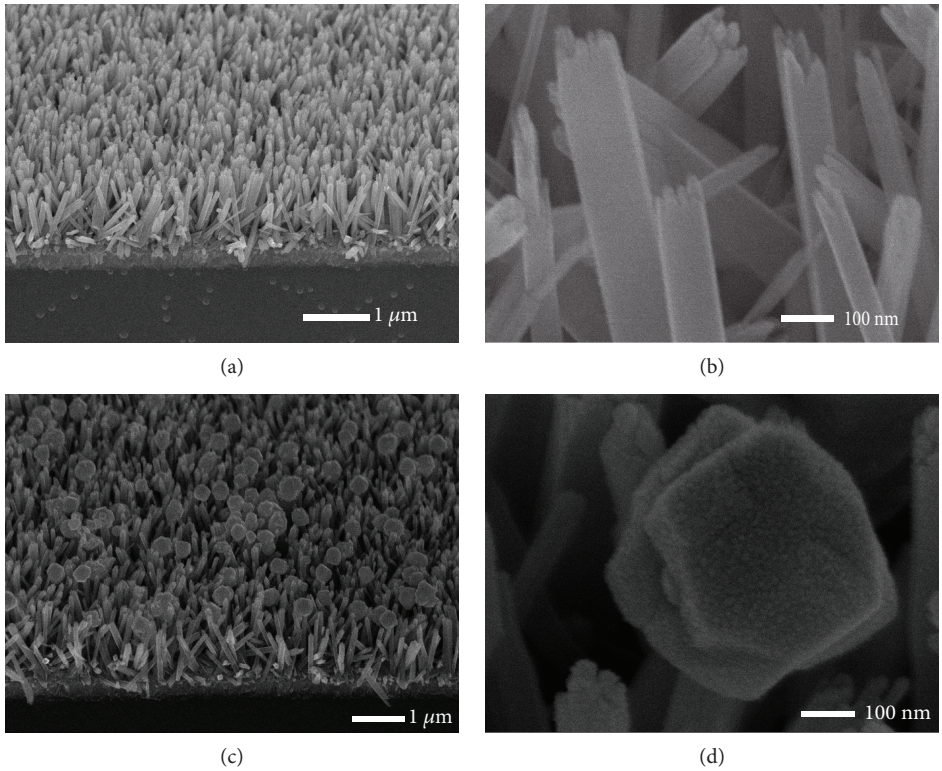

Figure 1: (a, b) SEM images of TiO_2 NR arrays. (c) SEM images of TiO_2/PbS deposited by electrochemistry for 20 min. (d) SEM images of the top of TiO_2/PbS.

heterostructures (the lattice ratio between CdS and PbS is 0.697). Due to the existence of the CdS interlayer, the fill factor and short current density of the photoanodes were greatly improved.

2. Experimental

2.1. Preparation of TiO_2 NR Arrays. TiO_2 NR arrays were fabricated through a hydrothermal synthesis [27, 39]. After mixing deionized water and concentrated hydrochloric acid (mass fraction 36.5-38%) of 60 mL each, 2 mL of titanium butoxide was added drop by drop into the solution under vigorous stirring at room temperature. A half hour later, 30 mL of the prepared precursor solution was transferred into a 100 mL stainless steel autoclave with a Teflon liner. And then, three pieces of FTO substrates which had been ultrasonically cleaned by a mixed solution (chloroform, acetone, and 2-propanol with a volume ratio of 1 : 1 : 1) for 60 min were placed with an angle against the wall (the conductive sides faced down) in the Teflon liner. The hydrothermal synthesis took place at 140°C for 14 h. When the autoclave was cooled to room temperature, the substrates were taken out, rinsed with deionized water, and dried in an oven at 150°C.

2.2. Preparation of TiO_2/PbS Heterostructures. The preparation of the TiO_2/PbS heterostructure was carried out by electrodeposition with a three-electrode system. A Pt sheet, a standard Ag/AgCl electrode, and the TiO_2 NR arrays on FTO (4.5 cm^2 working area) were used as the counter electrode, the reference electrode, and the working electrode, respectively. An electrolyte containing 0.1 M of $Pb(NO_3)_2$ and 0.1 M of thiourea in dimethyl sulphoxide (DMSO)/water (a volume ratio of 1 : 1) was kept at 90°C. After depositions from 2 to 30 min with a constant voltage of 0.5 V, the samples were taken out and washed with deionized water and ethanol, respectively.

2.3. Preparation of TiO_2/CdS Heterostructures. The preparation of the TiO_2/CdS heterostructure was carried out by electrodeposition with the same three-electrode system stated above. An electrolyte containing 0.2 M of $Cd(NO_3)_2$ and 0.2 M of thiourea in dimethyl sulphoxide (DMSO)/water (volume ratio of 1 : 1) was kept at 90°C. After depositions from 2 to 30 min with a constant voltage of 0.66 V, the samples were taken out and washed with deionized water and ethanol, respectively.

2.4. Preparation of TiO_2/CdS/PbS Heterostructures. The preparation of the TiO_2/PbS/CdS heterostructure was formed in two steps. (1) Following Section 2.3, the TiO_2/CdS heterostructure was firstly fabricated. (2) Following Section 2.2, PbS QDs were deposited over TiO_2/CdS nanocables.

2.5. Characterizations. Field emission scanning electron microscopy (FESEM, JEOL JSM-6700) was used to examine the microstructures of the samples. Transmission electron microscope (TEM) and high-resolution TEM (HRTEM) images of TiO_2/CdS heterostructures were taken by a JEM-2100F high-resolution transmission microscope. The absorption characterizations of all samples were measured

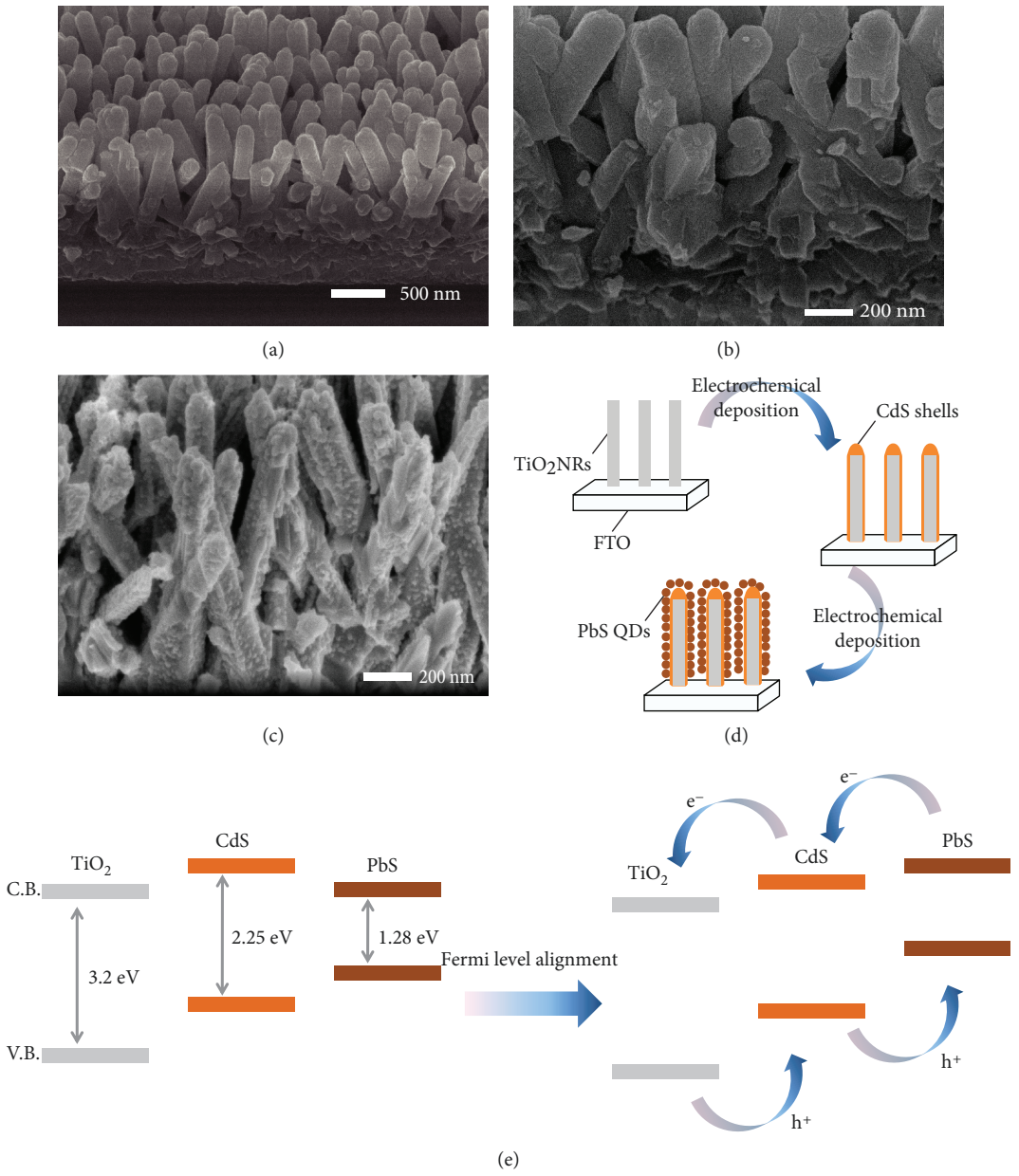

FIGURE 2: (a, b) SEM images of TiO_2/CdS nanocable arrays. (c) SEM image of TiO_2/CdS/Pb. (d) Schematic diagram of the growth process of the TiO_2/CdS/PbS heterostructures. (e) Relative band edges of TiO_2, CdS, and PbS (left) and the proposed band edges of TiO_2/CdS/PbS termed by Fermi level alignment (right).

with a UV-3150 spectrophotometer. A Rigaku D/max-2500 X-ray diffractometer (XRD) with Cu Kα radiation ($\lambda = 0.15418$ nm) was used at room temperature to analyze the crystal structures of TiO_2 and CdS. With an electrochemical workstation (Corrtest CS150), photoelectrochemical properties were tested under the three-electrode system where the samples, Pt sheet, and Ag/AgCl electrode worked as the working electrode, counter electrode, and reference electrode, respectively, in a polysulfide redox couple (S^{2-}/SO_3^{2-}) electrolyte (0.25 M Na_2S and 0.35 M Na_2SO_3 in deionized water), while a Zolix SS150 Solar Simulator was used as the illumination source with a power of 100 mW/cm^2.

3. Results and Discussion

3.1. TiO_2/PbS Heterostructures. Vertical TiO_2 NR arrays fabricated on FTO by hydrothermal synthesis are shown in Figure 1(a). The TiO_2 NRs grew orderly with a quadrangular prism morphology indicating well-crystallized structures. Their sides were very neat and smooth, which were different from their rugged tops (Figure 1(b)). Therefore, there were a lot of lattice defects at the tops. These NRs were about 2 μm long, and we could count that the planar density was 8-12 NRs per μm^2.

With these as-prepared TiO_2 NRs, PbS was deposited electrochemically, and the SEM images show the morphologies of

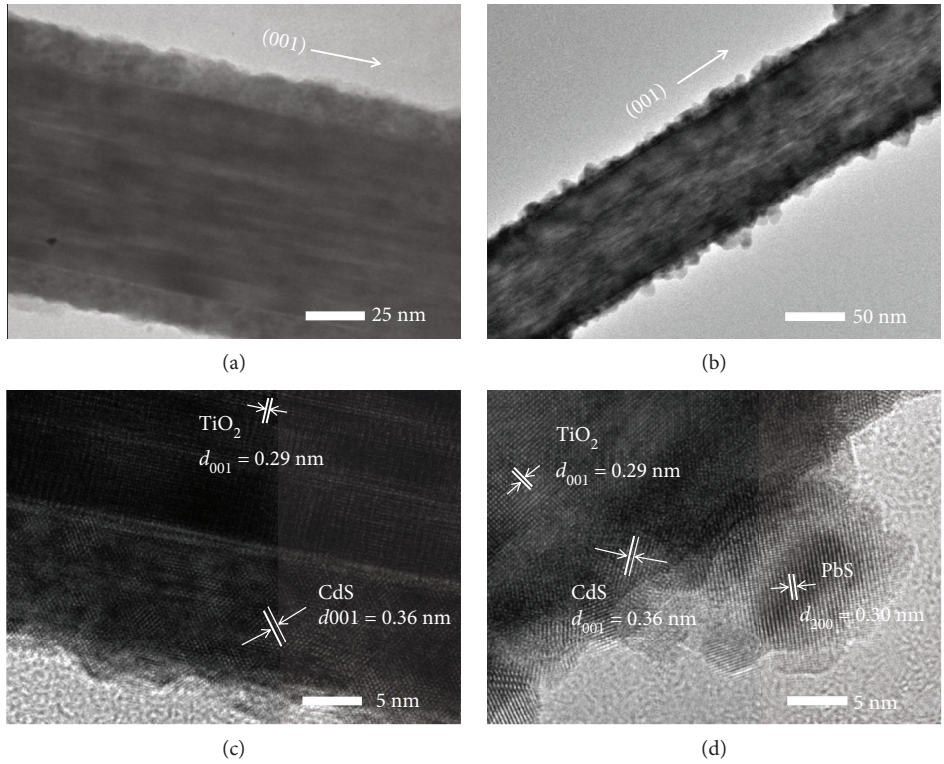

Figure 3: (a) TEM image of a TiO_2 NR coated with a CdS shell. (b) TEM image of TiO_2/CdS/PbS. (c) HRTEM image shows the interface and crystalline structure of TiO_2/CdS. (d) HRTEM image shows the interface and crystalline structure of TiO_2/CdS/PbS.

samples deposited for 20 min (Figures 1(c) and 1(d)). In Figure 1(c), it is clear to see that the quadrangular prism NRs were covered by PbS NPs (diameter around 300 nm) which were obviously distinguished in the SEM image over the top of the TiO_2 NRs.

3.2. TiO_2/CdS/PbS Heterostructures. The CdS/PbS heterostructure has already been widely used in the areas of photovoltaic and photocatalysis. Here, we would insert a CdS layer between TiO_2 and PbS to fabricate TiO_2/CdS/PbS heterostructures for our photoanodes.

With the as-prepared TiO_2 NRs, CdS was firstly deposited by the electrochemical method. Figures 2(a) and 2(b) show the morphologies of samples deposited with CdS for 30 min. The morphologies of the NRs changed from quadrangular prisms to cylinders whose diameters became ~50 nm larger, and the surface was no longer smooth. In Figure 2(b), it is clear to see that the quadrangular prism NRs were covered by CdS shells which were easily distinguished in the SEM image. Comparing with the smooth sides of TiO_2 NRs, there were more defect centers which could be good for the epitaxial growth.

Furthermore, we deposited PbS over the prepared TiO_2/CdS nanocables at the same conditions. In Figure 2(c), the SEM image shows the morphology of the sample deposited with CdS for 10 min and PbS for 10 min. It is clear to see that there are dense PbS QDs adhered all over the TiO_2/CdS nanocables. Through these observations, the growth process is summarized in Figure 2(d). CdS grew over the surface of TiO_2 NRs, and the core/shell TiO_2/CdS structures were

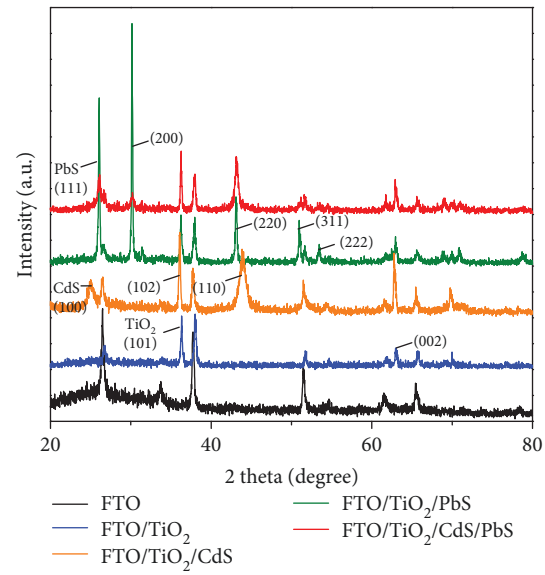

Figure 4: XRD patterns of FTO (black line), TiO_2 NRs (blue line), TiO_2/CdS (orange line), TiO_2/PbS (green line), and TiO_2/CdS/PbS (red line).

formed. The relative band edges of TiO_2, CdS, and PbS are shown in Figure 2(e) with their band gaps, respectively, to be 3.20, 2.25, and 1.28 eV. When the TiO_2/CdS/PbS heterostructure is formed, their band edges at the interfaces would be termed by Fermi level alignment shown in the right part of Figure 2(e).

The core/shell rod structure (nanocable) could also be seen from the TEM image with CdS deposited for 15 min (Figure 3(a)), while in the HRTEM image (Figure 3(c)) it is easy to distinguish the interface between TiO_2 core and CdS shell and the d spacings of TiO_2 (001) and CdS (100) were 0.29 nm and 0.36 nm, respectively. In Figure 3(b), it shows the TEM image of TiO_2/CdS/PbS QDs deposited with CdS for 10 min and PbS for 10 min. Except the d spacings of TiO_2 (001) and CdS (100), the d spacing of PbS (200) is shown to be 0.30 nm (Figure 3(d)).

3.3. Phase Composition and Structure. In Figure 4, there are two new peaks of the XRD pattern of TiO_2 NRs (blue line) compared with the pattern of FTO (black line), and the two peaks, respectively, correspond to the different planes of tetragonal phase rutile TiO_2 (JCPDS 88-1175) exhibited as quadrangular prisms in the SEM images. The two predominant peaks at 36.4° and 63.2°, respectively, indexed to the (101) and (002) planes suggesting that the growth of the TiO_2 NRs took place along their c-axis on the FTO substrate proved in Figure 1(a). When CdS was electrochemically deposited (shell), two new diffraction peaks (orange line) appeared at 24.84° and 43.74° which, respectively, indexed to the (100) and (110) planes of the hexagonal CdS (JCPDS 77-2306). Meanwhile, the intensity of the peak around 36° was higher, because this peak was not only from the (101) plane of the tetragonal TiO_2 but also from the (102) plane of the hexagonal CdS. When PbS was deposited (nanoparticle), there were several new diffraction peaks (green line) that appeared at 25.96°, 30.07°, 43.06°, 50.76°, and 53.41° which, respectively, indexed to the (111), (200), (220), (311), and (222) planes of the galena PbS (JCPDS 05-0592). The red line represents the XRD pattern of the TiO_2/CdS/PbS heterostructure, and the typical peaks of all components could be found.

3.4. Morphologies Controlled by the Lattice Ratio. From the SEM and TEM images, TiO_2 NRs grew along the [001] direction. The lattice constants of the TiO_2 NRs (JCPDS 88-1175) and PbS NPs (JCPDS 05-0592) shown in Table 1 are, respectively, $a = b = 0.4517$ nm, $c = 0.294$ nm, and $a = b = c = 0.5936$ nm. At the sides of the TiO_2 NRs, the lattice ratio between TiO_2 ($c = 0.294$ nm) and PbS ($a = b = c = 0.5936$ nm) is 0.495. At the top of TiO_2 NRs, the lattice ratio between TiO_2 ($a = b = 0.4517$ nm) and PbS ($a = b = c = 0.5936$ nm) is 0.761. Therefore, PbS NPs were deposited on the top of TiO_2 NRs.

Proved from the XRD pattern, the lattice constants of the CdS (JCPDS 77-2306) shown in Table 1 are $a = b = 0.4136$ nm, $c = 0.6713$ nm. The lattice ratio between TiO_2 ($a = 0.4517$ nm) and CdS ($a = b = 0.4136$ nm) is 0.916. Because of the high lattice ratio, CdS could be deposited all over the TiO_2 nanorods and the core/shell TiO_2/CdS nanocables were therefore formed. The lattice ratio between CdS ($a = b = 0.4136$ nm) and PbS ($a = b = c = 0.5936$ nm) is 0.697, so PbS could easily deposit on CdS.

3.5. UV-Vis Absorption. The UV-Vis absorption spectra of all samples with different treatments are shown in Figure 5.

Table 1: Lattice constants of TiO_2, CdS, and PbS.

Lattice constant	a (nm)	b (nm)	c (nm)
TiO_2	0.4517	0.4517	0.294
CdS	0.4163	0.4163	0.6713
PbS	0.5936	0.5936	0.5936

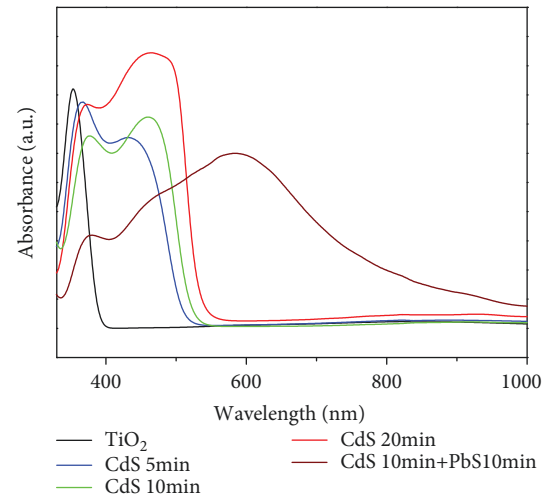

Figure 5: UV-Vis absorption spectra of TiO_2 NRs (black line); TiO_2/CdS deposited with CdS for 5 min (blue line), 10 min (green line), and 20 min (red line); and TiO_2/CdS/PbS deposited with CdS for 10 min and PbS for 10 min (wine line). The electrolyte for CdS contained 0.2 M of $Cd(NO_3)_2$ and 0.2 M of thiourea; the electrolyte or PbS contained 0.1 M of $Cd(NO_3)_2$ and 0.1 M of thiourea.

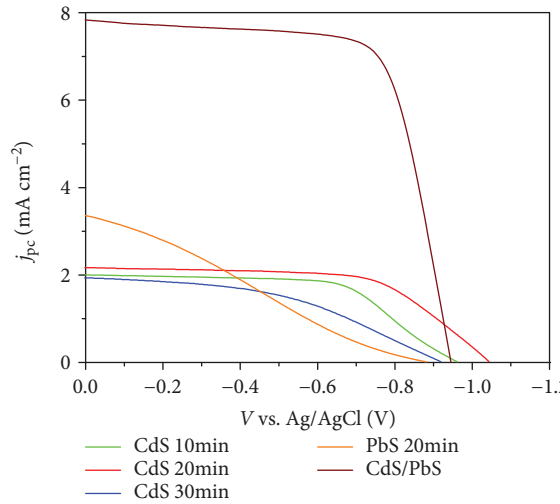

Figure 6: Photocurrent density-output potential difference (J-V) curves of TiO_2/CdS deposited with CdS for 10 min (green line), 20 min (red line), and 30 min (blue line); TiO_2/PbS deposited with PbS for 20 min (orange line); and TiO_2/CdS/PbS deposited with CdS for 20 min and PbS for 20 min (wine line).

Comparing the black line (TiO_2) and the blue line (deposited with CdS for 5 min), it is clear to see that the absorption range was broadened from the UV region to the visible light region

Table 2: Photovoltage characteristics of photoanodes.

Sample	Photocurrent density (mA cm^{-2})	Output potential difference V vs. Ag/AgCl (V)	Fill factor
CdS 10 min	2.04	0.98	0.57
CdS 20 min	2.17	1.03	0.62
CdS 30 min	1.92	0.92	0.42
PbS 10 min	3.36	0.90	0.26
CdS 10 min + PbS 10 min	7.83	0.94	0.63

with CdS over TiO_2 NRs. Comparing the blue line (deposited with CdS for 5 min) to the green (deposited with CdS for 10 min) and red lines (deposited with CdS for 20 min), the absorption ranges of TiO_2/CdS were further broadened with the increase in deposition time (more CdS). When PbS was deposited, the absorption range was extended to the near infrared region shown as the wine line. With a larger area of absorption range, the photoanode could be excited by more photons and a higher short current density would be achieved.

3.6. Photovoltaic Performance of the Electrodes. In Figure 6, it shows the photocurrent density-output potential difference (J-V) curves of the photoanodes fabricated by different conditions. When PbS was deposited over TiO_2 NRs (orange line), the photovoltage characteristics are given in Table 2 with the photocurrent density, output potential difference, and fill factor, respectively, to be 3.36 mA cm^{-2}, 0.90 V, and 0.26. The rather low fill factor was consistent with the SEM images that PbS NPs just grew on the top of TiO_2 NRs and they did not grow on the sides. Shown in Figure 6 and Table 1, the photocurrent density of TiO_2/CdS increased at first and then decreased and the output potential differences had no obvious change with more CdS deposition time. The highest photocurrent density of TiO_2/CdS was 2.17 mA cm^{-2} when CdS was deposited for 20 min. After TiO_2/CdS/PbS formed, the absorption range was broadened and PbS NPs densely covered all over the nanocables. Thus, it is clear to see that the photocurrent density and fill factor were largely increased from 3.36 mA cm^{-2} to 7.83 mA cm^{-2} and from 0.26 to 0.63 (Figure 6 and Table 2).

4. Conclusions

With a suitable lattice distance between PbS and TiO_2, CdS was selected to coat on the surface of TiO_2 nanorods and then PbS QDs were epitaxially grown all over the surface of TiO_2/CdS nanocables to form a TiO_2/CdS/PbS heterostructure. This strategy solves the difficulty to directly grow PbS QDs on TiO_2 NR arrays and makes use of the optoelectronic property of PbS QDs for superior photovoltage characteristics of the TiO_2/CdS/PbS photoanode.

Data Availability

The data used to support the findings of this study are available from the corresponding author upon request.

Conflicts of Interest

There is no conflict of interest.

Acknowledgments

This work was supported by the National Natural Science Foundation of China (51772123 and 11674127), Jilin Province Science Fund for Excellent Young Scholars (20170520129JH), and Board of Regents Support Funds Professorship.

References

[1] G. Wei, S. Wang, K. Renshaw, M. E. Thompson, and S. R. Forrest, "Solution-processed squaraine bulk heterojunction photovoltaic cells," *ACS Nano*, vol. 4, no. 4, pp. 1927–1934, 2010.

[2] D. A. R. Barkhouse, A. G. Pattantyus-Abraham, L. Levina, and E. H. Sargent, "Thiols passivate recombination centers in colloidal quantum dots leading to enhanced photovoltaic device efficiency," *ACS Nano*, vol. 2, no. 11, pp. 2356–2362, 2008.

[3] A. A. Bakulin, S. Neutzner, H. J. Bakker, L. Ottaviani, D. Barakel, and Z. Chen, "Charge trapping dynamics in PbS colloidal quantum dot photovoltaic devices," *ACS Nano*, vol. 7, no. 10, pp. 8771–8779, 2013.

[4] M. T. Rizi and M. H. Shahrokh Abadi, "Numerical investigation on efficiency improvement of double layer antireflection coating AZO/buffer/Cu_2O/CuO on back-surface fluorine-doped tin oxide heterostructure solar cells," *Journal of the Optical Society of America B*, vol. 36, no. 4, pp. 1155–1165, 2019.

[5] S. R. Rosario, I. Kulandaisamy, A. M. S. Arulanantham et al., "Fabrication and characterization of lead sulfide (PbS) thin film based heterostructure (FTO/CdS/PbS/Ag) solar cell by nebulizer spray method," *Materials Research Express*, vol. 6, no. 5, 2019.

[6] S. Kumar, S. Khanchandani, M. Thirumal, and A. K. Ganguli, "Achieving enhanced visible-light-driven photocatalysis using type-II $NaNbO_3$/CdS core/shell heterostructures," *ACS Applied Materials & Interfaces*, vol. 6, no. 15, pp. 13221–13233, 2014.

[7] W. J. Lee, J. M. Lee, S. T. Kochuveedu et al., "Biomineralized N-doped CNT/TiO_2 core/shell nanowires for visible light photocatalysis," *ACS Nano*, vol. 6, no. 1, pp. 935–943, 2012.

[8] D. R. Baker and P. V. Kamat, "Photosensitization of TiO_2 nanostructures with CdS quantum dots: particulate versus tubular support architectures," *Advanced Functional Materials*, vol. 19, no. 5, pp. 805–811, 2009.

[9] N. N. Hewa-Kasakarage, M. Kirsanova, A. Nemchinov et al., "Radiative recombination of spatially extended excitons in (ZnSe/CdS)/CdS heterostructured nanorods," *Journal of the American Chemical Society*, vol. 131, no. 3, pp. 1328–1334, 2009.

[10] P. Brown and P. V. Kamat, "Quantum dot solar cells. Electrophoretic deposition of CdSe–C_{60} composite films and capture of photogenerated electrons with nC_{60} cluster shell," *Journal of*

the American Chemical Society, vol. 130, no. 28, pp. 8890-8891, 2008.

[11] K. S. Leschkies, R. Divakar, J. Basu et al., "Photosensitization of ZnO nanowires with CdSe quantum dots for photovoltaic devices," *Nano Letters*, vol. 7, no. 6, pp. 1793–1798, 2007.

[12] X. Wang, H. Zhu, Y. Xu et al., "Aligned ZnO/CdTe core–shell nanocable arrays on indium tin oxide: synthesis and photoelectrochemical properties," *ACS Nano*, vol. 4, no. 6, pp. 3302–3308, 2010.

[13] R. Plass, S. Pelet, J. Krueger, M. Grätzel, and U. Bach, "Quantum dot sensitization of organic–inorganic hybrid solar cells," *The Journal of Physical Chemistry B*, vol. 106, no. 31, pp. 7578–7580, 2002.

[14] W. Ma, S. L. Swisher, T. Ewers et al., "Photovoltaic performance of ultrasmall PbSe quantum dots," *ACS Nano*, vol. 5, no. 10, pp. 8140–8147, 2011.

[15] X. Zhang, Y. Zhang, L. Yan et al., "High photocurrent PbSe solar cells with thin active layers," *Journal of Materials Chemistry A*, vol. 3, no. 16, pp. 8501–8507, 2015.

[16] X. Zhang, Y. Zhang, L. Yan et al., "PbSe nanocrystal solar cells using bandgap engineering," *RSC Advances*, vol. 5, no. 80, pp. 65569–65574, 2015.

[17] X. Zhang, Y. Zhang, H. Wu et al., "PbSe quantum dot films with enhanced electron mobility employed in hybrid polymer/nanocrystal solar cells," *RSC Advances*, vol. 6, no. 21, pp. 17029–17035, 2016.

[18] H. Wu, X. Zhang, Y. Zhang et al., "Colloidal PbSe solar cells with molybdenum oxide modified graphene anodes," *ACS Applied Materials & Interfaces*, vol. 7, no. 38, pp. 21082–21088, 2015.

[19] C. Ji, Y. Zhang, X. Zhang et al., "Paper synthesis and characterization of $Ag_2S_xSe_{1-x}$ nanocrystals and their photoelectrochemical property," *Nanotechnology*, vol. 28, no. 6, article 065602, 2017.

[20] L. Etgar, T. Moehl, S. Gabriel, S. G. Hickey, A. Eychmüller, and M. Grätzel, "Light energy conversion by mesoscopic PbS quantum dots/TiO_2 heterojunction solar cells," *ACS Nano*, vol. 6, no. 4, pp. 3092–3099, 2012.

[21] J. J. Wu and C. C. Yu, "Aligned TiO_2 nanorods and nanowalls," *The Journal of Physical Chemistry B*, vol. 108, no. 11, pp. 3377–3379, 2004.

[22] D. Kuang, J. Brillet, P. Chen et al., "Application of highly ordered TiO_2 nanotube arrays in flexible dye-sensitized solar cells," *ACS Nano*, vol. 2, no. 6, pp. 1113–1116, 2008.

[23] A. K. Chandiran, M. Abdi-Jalebi, M. K. Nazeeruddin, and M. Grätzel, "Analysis of electron transfer properties of ZnO and TiO_2 photoanodes for dye-sensitized solar cells," *ACS Nano*, vol. 8, no. 3, pp. 2261–2268, 2014.

[24] M. Law, L. E. Greene, A. Radenovic, T. Kuykendall, J. Liphardt, and P. Yang, "ZnO–Al_2O_3 and ZnO–TiO_2 core–shell nanowire dye-sensitized solar cells," *The Journal of Physical Chemistry B*, vol. 110, no. 45, pp. 22652–22663, 2006.

[25] B. Carlson, K. Leschkies, E. S. Aydil, and X.-Y. Zhu, "Valence band alignment at cadmium selenide quantum dot and zinc oxide $(10\bar{1}0)$ interfaces," *The Journal of Physical Chemistry C*, vol. 112, no. 22, pp. 8419–8423, 2008.

[26] X. Y. Yu, J. Y. Liao, K. Q. Qiu, D. B. Kuang, and C. Y. Su, "Dynamic study of highly efficient CdS/CdSe quantum dot-sensitized solar cells fabricated by electrodeposition," *ACS Nano*, vol. 5, no. 12, pp. 9494–9500, 2011.

[27] P. Wang, Y. Zhang, L. Su et al., "Photoelectrochemical properties of CdS/CdSe sensitized TiO_2 nanocable arrays," *Electrochimica Acta*, vol. 165, pp. 110–115, 2015.

[28] C. H. Chang and Y. L. Lee, "Chemical bath deposition of CdS quantum dots onto mesoscopic TiO_2 films for application in quantum-dot-sensitized solar cells," *Applied Physics Letters*, vol. 91, no. 5, article 053503, 2007.

[29] S. Gimenez, T. Lana-Villarreal, R. Gomez, S. Agouram, V. Munoz-Sanjose, and I. Mora-Sero, "Determination of limiting factors of photovoltaic efficiency in quantum dot sensitized solar cells: correlation between cell performance and structural properties," *Journal of Applied Physics*, vol. 108, no. 6, article 064310, 2010.

[30] B. Farrow and P. V. Kamat, "CdSe quantum dot sensitized solar cells. Shuttling electrons through stacked carbon nanocups," *Journal of the American Chemical Society*, vol. 131, no. 31, pp. 11124–11131, 2009.

[31] H. J. Lee, M. Wang, P. Chen et al., "Efficient CdSe quantum dot-sensitized solar cells prepared by an improved successive ionic layer adsorption and reaction process," *Nano Letters*, vol. 9, no. 12, pp. 4221–4227, 2009.

[32] L. J. Diguna, Q. Shen, J. Kobayashi, and T. Toyoda, "High efficiency of CdSe quantum-dot-sensitized TiO_2 inverse opal solar cells," *Applied Physics Letters*, vol. 91, no. 2, article 023116, 2007.

[33] Y. Chen, X. Zhang, Q. Tao et al., "High catalytic activity of a PbS counter electrode prepared via chemical bath deposition for quantum dots-sensitized solar cells," *RSC Advances*, vol. 5, no. 3, pp. 1835–1840, 2015.

[34] S. S. Mali, S. K. Desai, S. S. Kalagi et al., "PbS quantum dot sensitized anatase TiO_2 nanocorals for quantum dot-sensitized solar cell applications," *Dalton Transactions*, vol. 41, no. 20, pp. 6130–6136, 2012.

[35] A. H. Ip, S. M. Thon, S. Hoogland et al., "Hybrid passivated colloidal quantum dot solids," *Nature Nanotechnology*, vol. 7, no. 9, pp. 577–582, 2012.

[36] A. G. Pattantyus-Abraham, I. J. Kramer, A. R. Barkhouse et al., "Depleted-heterojunction colloidal quantum dot solar cells," *ACS Nano*, vol. 4, no. 6, pp. 3374–3380, 2010.

[37] H. J. Lee, H. C. Leventis, S.-J. Moon et al., "PbS and CdS quantum dot-sensitized solid-state solar cells: "old concepts, new results"," *Advanced Functional Materials*, vol. 19, no. 17, pp. 2735–2742, 2009.

[38] J. Hernández-Borja, Y. V. Vorobiev, and R. Ramírez-Bon, "Thin film solar cells of CdS/PbS chemically deposited by an ammonia-free process," *Solar Energy Materials and Solar Cells*, vol. 95, no. 7, pp. 1882–1888, 2011.

[39] B. Liu and E. S. Aydil, "Growth of oriented single-crystalline rutile TiO_2 nanorods on transparent conducting substrates for dye-sensitized solar cells," *Journal of the American Chemical Society*, vol. 131, no. 11, pp. 3985–3990, 2009.